Rare Metal Materials and Engineering
Volume 49, Issue 2, February 2020
Available online at www.rmme.ac.cn

Science Press

Cite this article as: Rare Metal Materials and Engineering, 2020, 49(2): 0435-0440.

ARTICLE

Influence of Pt:Ni Atomic Ratio on Oxygen Reduction Reaction Activities of Pt-Ni Octahedral Nanoparticles

Duan Xiao[1], Huang Long[1], Li Yunyan[1], Tang Ling[1], Lu Jun[1], Zhao Yunkun[2], Liu Feng[1]

[1] Sino-Precious Metals Holding Co, Ltd., Kunming 650106, China; [2] State-Local Joint Engineering Laboratory of Precious Metal Catalytic Technology and Application, Kunming Sino-Platinum Metals Catalysts Co., Ltd, Kunming 650106, China

Abstract: Octahedral Pt-Ni nanoparticles are considered as promising catalysts for oxygen reduction reaction (ORR). The relationship between the Pt:Ni atomic ratio and the corresponding ORR activity is presented as a volcano plot without explanation. Herein, by studying the ORR performance of Pt-Ni octahedral nanoparticles with different Pt:Ni atomic ratios, an abnormal trend of ORR specific activities in the order of Pt_3Ni>$PtNi_2$>PtNi was found. Meanwhile, with the same Pt loading, the sequence of ORR mass activity is Pt_3Ni≈$PtNi_2$>PtNi. The degree of surface lattice contraction and the utilization of Pt were considered to account for these phenomena. The extent of surface lattice contraction is decreased as Pt_3Ni>$PtNi_2$>PtNi, consistent with the sequence of ORR specific activity. While the mass activity is affected by both the specific activity and the surface Pt utilization. The results indicate that the ORR activity can be adjusted by tuning the surface tension and the surface Pt utilization.

Key words: oxygen reduction reaction; Pt-Ni octahedron; atomic ratio; surface lattice contraction; Pt utilization

Proton exchange membrane fuel cells (PEMFCs) are potential alternative to fossil energy powering devices due to their advantages such as high efficiency, quiet working condition and no pollution. However, the commercialization of PEMFCs was hindered by the sluggish kinetic of cathodic oxygen reduction reaction (ORR). Pt-based alloy nanoparticles consisting of Pt and 3d transition metals (such as Fe, Co, Ni and Cu)[1-11] are considered as promising catalyst for ORR. The pioneering work by Stamenkovic et al confirmed that Pt_3Ni (111) plane shows extremely high activity towards ORR, being 90 times more active than that of Pt/C[12]. Since then, numerous effects have been focused on synthesizing Pt-Ni octahedral nanoparticles with (111) facet[4,13,14]. Cui et al[4] reported the synthesis of Pt-Ni octahedral nanoparticles with high ORR activity, which was varied with Pt:Ni ratio, but no detailed explanation was given. Herein, we synthesized Pt-Ni octahedral nanoparticles with different Pt:Ni ratios according to the method developed by Cui and co-workers[4]. The ORR activities of as-synthesized Pt_3Ni (Pt 66 at%), PtNi (Pt 47 at%), $PtNi_2$ (Pt 27 at%) octahedral nanoparticles were compared. The results indicated that the relationship between ORR activity and Pt:Ni atomic ratio does not agree with the previous reports. The crystal structure and near-surface composition of the nanoparticles were studied to explain the abnormal phenomenon.

1 Experiment

1.1 Synthesis of Pt-Ni octahedral nanoparticles with different atomic ratios

In a typical synthesis developed by Cui and co-workers[14], $Pt(acac)_2$ and $Ni(acac)_2$ were dissolved and mixed in 50 mL N,N-dimethylformamide (DMF), the total molar concentration of precursors was 8 mmol/L (for Pt_3Ni: 4 mmol/L $Pt(acac)_2$, 4 mmol/L $Ni(acac)_2$; for PtNi: 2.2 mmol/L $Pt(acac)_2$, 5.8 mmol/L $Ni(acac)_2$; for $PtNi_2$: 2 mmol/L $Pt(acac)_2$, 6 mmol/L $Ni(acac)_2$). The solution was transferred to a PTFE-lined autoclave. Then the sealed autoclave was heated from room temperature to 120 °C within 10 min (held at 120 °C, 42 h).

Received date: February 21, 2019
Foundation item: National Key Research and Development Program of China (2016YFB0101309); Kunming Science and Technology Plan Project (2015-1-G-01001)
Corresponding author: Liu Feng, Ph. D., Sino-Precious Metals Holding Co., Ltd, Kunming 650106, P. R. China, Tel: 0086-871-68316562, E-mail: feng.liu@spmcatalyst.com

Copyright © 2020, Northwest Institute for Nonferrous Metal Research. Published by Science Press. All rights reserved.

Cooling down to room temperature before it was washed with ethanol/water several times and mixed with carbon support (Vulcan XC-72) to form Pt-Ni/C (Pt loading was 30 wt% for all Pt-Ni/C catalyst). The as-synthesized Pt-Ni/C catalysts were then dried under vacuum at 60 °C for 6 h.

1.2 Electrochemical measurements

The catalyst ink was prepared by dispersing 2.5 mg catalyst powder into a solution containing 1 mL ultrapure water (18.2 MΩ), 1 mL isopropanol and 15 μL of 5 wt% Nafion® solution. Then the suspension was ultrasonicated until homogenous ink was formed. A 20 μL aliquot of ink was dropped onto the rotating disk electrode (RDE) with Pt loading of ~25 μg/cm^2. The ink was dried under room temperature with rotating to form a uniform thin film at the RDE surface.

The electrochemical cell was designed to be three necks. RDE decorated with thin film catalysts layer was adopted as working electrode. A reversible hydrogen electrode (RHE) and a Pt plate electrode were used as reference electrode and counter electrode, respectively. All the potentials in this study refer to RHE. The electrochemical experiments were performed by workstation Autolab AUT85938 (Metrohm).

The working electrode was firstly activated by cyclic voltammetry between 0.02 V and 1.1 V in nitrogen-saturated 0.1 mol/L $HClO_4$ solution at a scanning rate of 50 mV/s for 20 cycles. The 19th potential cycle was selected to evaluate the electrochemical surface area (ECSA) of Pt.

Linear sweep voltammetry measurements were conducted in an oxygen-saturated 0.1 mol/L $HClO_4$ solution by sweeping the potential from 0.3 V to 1.01 V at a scanning rate of 20 mV/s with rotation speed of 1600 r/min. The kinetic current (I_k) can be calculated using the Koutecky-Levich equation[15] which is expressed by

$$\frac{1}{I}=\frac{1}{I_k}+\frac{1}{I_d} \quad (1)$$

where I is the measured current and I_d is the diffusion limited current. The I_d term can be obtained from the Levich equation[15]:

$$I_d = 0.62nFAD^{\frac{2}{3}}v^{\frac{-1}{6}}\omega^{\frac{1}{2}}C_{O_2} \quad (2)$$

where n is the number of electrons transferred; F is Faraday's constant (96 485 C/mol); A is the geometrical area of the electrode (0.196 cm^2); D is the diffusion coefficient of O_2 in 0.1 mol/L $HClO_4$ solution (1.93×10^{-5} cm^2/s); v is the kinematic viscosity of the electrolyte (1.01×10^{-2} cm^2/s); ω is the angular frequency of rotation, $\omega=2\pi f/60$, f is the RDE rotation rate in r/min and C_{O_2} is the concentration of molecular oxygen in 0.1 mol/L $HClO_4$ solution (1.26×10^{-6} mol/cm^3). The kinetic current densities at 0.9 V were selected as an index to evaluate the ORR performance.

1.3 Physical characterizations

Inductively coupled plasma optical emission spectroscopy (ICP-OES) was used to analyze the composition of as-synthesized catalysts. Dried catalyst powders were wet-ashed through perchloric acid ($HClO_4$ BDH Aristar Trace Metal grade), and analyzed by a Perkin Elmer Optima 8000 ICP-OES calibrated with an in-house prepared platinum standard with a concentration of approximately 3 mg/mL. The accuracy and precision of this analysis is within 1%~3% of the reported value on a relative basis.

X-ray diffraction (XRD) data was collected on a Rigaku Smart Lab 3~9 kW in a parallel-beam configuration using copper Kα radiation. Data were collected from 30° to 75° at a fixed incidence angle of 4° using a 0.04° step size and an integration time of 2 s/step. Phases were identified by comparing the observed data to reference data from the International Centre for Diffraction Data (ICDD). Lattice parameters were calculated from the diffraction peak angle using Bragg's Law.

Transmission electron microscopy (TEM) and high-resolution transmission electron microscopy (HRTEM) observation were performed on a JEOL JEM 2100 (200 kV). The sample was prepared by suspending the as-synthesized nanoparticles in ethanol solution and then dropped onto a carbon-coated copper grid, dried under an infrared light.

X-ray photoelectron spectroscopy (XPS) test was performed on a PHI5000 VersaProbe II spectrometer with the Mg Kα radiation (1253.6 eV) unmonochromatic Al Kα radiation (1486.6 eV), and the vacuum in the analysis chamber was maintained at about 0.9~1.0 kPa or lower, operating at 12.5 kV and 250 W. The surface charging effect was corrected by fixing the C_{1s} peak at a binding energy of 284.6 eV.

2 Results and Discussion

2.1 ORR activities of the as-synthesized Pt-Ni nanoparticles

The as-synthesized Pt-Ni nano-particles were supported on carbon black before they were loaded on RDE to evaluate their ORR activity. The loading of Pt on carbon supported catalysts was fixed at 30 wt%. The CV curves of three catalysts are listed in Fig.1a. The characterized adsorption and desorption peak of under-potential deposition hydrogen (HUPD) in the potential range between 0.02 V and 0.4 V indicates the surface of catalysts is free of Ni. The surface Ni is leaching during the electrochemical activation process. The ECSA can be calculated by integrating the charge corresponding to desorption of HUPD assuming a specific charge of 210 μC/cm$^2_{Pt}$ [16]. The curves of ORR polarization are shown in Fig.1b. As can be seen, all the as-synthesized Pt-Ni nanoparticles show better ORR activity than commercial Pt/C since the half-wave potential is positively shifted. The corresponding Tafel curves in Fig.1c and 1d further confirm the superior ORR activity for the as-synthesized Pt-Ni nanocatalysts. The kinetic current of ORR was calculated according to Eq. (1) and (2), and then the kinetic current was further normalized to mass and ECSA of Pt, obtaining mass current density (j_m) and specific current density (j_s), respectively. The values of j_m and

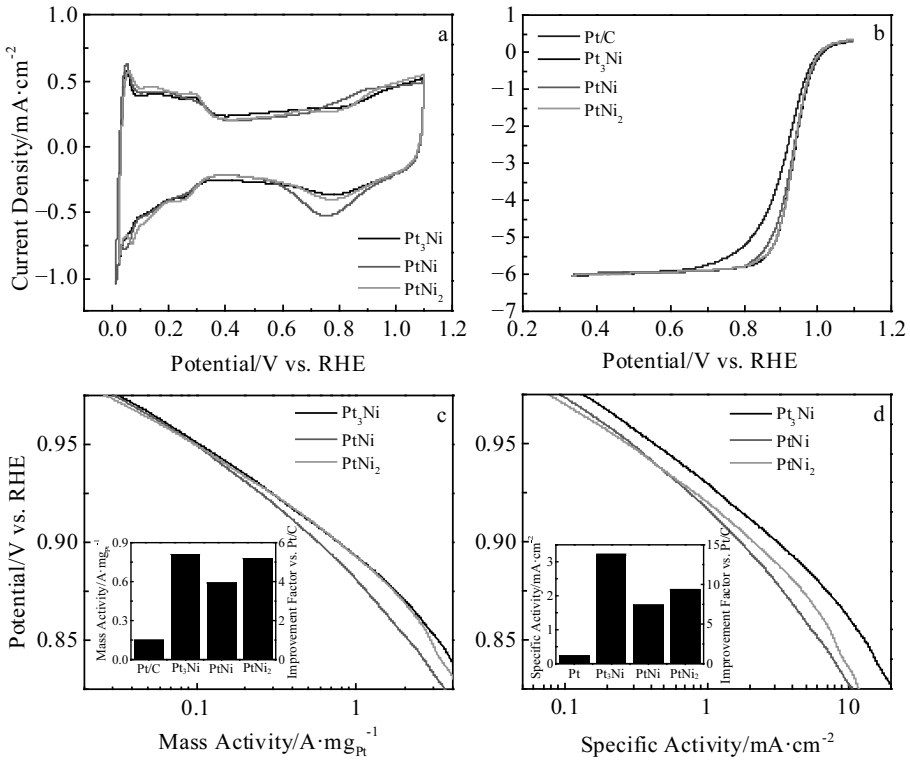

Fig.1 RDE characterization of PtNi nanoparticles synthesized with different Pt:Ni atomic ratios: (a) cyclic voltammograms of the catalysts in N_2-saturated 0.1 mol/L $HClO_4$ at 25 °C (50 mV/s), (b) ORR polarization curves in O_2-saturated 0.1 mol/L $HClO_4$ at 25 °C and 1600 r/min (20 mV/s), and (c, d) mass activity and specific activity of different PtNi nanoparticles (insets show the activity of the reference commercial Pt/C at 0.9 V)

j_s at 0.9 V on as-synthesized nanocatalysts and commercial Pt/C are compared as inserted in Fig.1c and 1d. It is clear that the specific ORR activity of as-synthesized Pt-Ni nanocatalysts at 0.9 V is 7~14 times as high as that on commercial Pt/C, while the Pt mass activity is enhanced by a factor of 4~5.4.

Notice that, both j_m and j_s are varied with Pt:Ni atomic ratio. A volcano plot relationship between the Pt:Ni atomic ratio and the corresponding j_m and j_s value has been reported before[17]. However, neither j_m nor j_s follows that volcano plot trend here. As shown in insets of Fig.1c and 1d, the relationship between the Pt:Ni atomic ratio and the corresponding ORR activity is shaped as a "crater plot". PtNi/C, with an intermediate Pt:Ni atomic ratio, shows the poorest ORR activity among the three Pt-Ni/C nanocatalysts.

2.2 Structural characterization of the as-synthesized Pt-Ni nanoparticles

To explain the unconventional crater plot relationship between the Pt:Ni atomic ratio and the corresponding ORR activity, TEM and X-ray diffraction (XRD) were applied to analyze the morphology and structure of the as-synthesized Pt-Ni nanoparticles. Fig.2 shows the typical transmission electron microscopy (TEM) images of as-synthesized Pt-Ni nanoparticles with different Pt:Ni atomic ratios. It is clear that most of nanoparticles are in octahedral morphology. The results of high-resolution transmission electron microscopy (HRTEM) further confirm that the as-synthesized Pt-Ni nanoparticles are surrounded by (111) facet. The *d*-spacing of as-synthesized Pt-Ni nanoparticles varies with the Pt:Ni atomic ratio. For Pt_3Ni, PtNi and $PtNi_2$, the *d*-spacing are measured to be 0.213, 0.220 and 0.216 nm, respectively. All the *d*-spacing values of as-synthesized Pt-Ni octahedral nanoparticles are smaller than that of Pt (111) (0.229 nm), indicating crystal contraction due to the incorporation of smaller Ni atom into the Pt lattice. The average particle size of as-synthesized Pt_3Ni, PtNi and $PtNi_2$ octahedral is 8.02 ± 1.48, 5.00 ± 0.84 and 7.90 ± 1.89 nm, respectively. Since the as-synthesized Pt-Ni nanoparticles are all in octahedral shape, it is clear that the *d*-spacing and the particle size are influenced by the Pt:Ni atomic ratio.

The XRD patterns of as-synthesized Pt-Ni octahedral nanoparticles are shown in Fig.3a, and the vertical line on the bottom corresponding to the XRD patterns is standard sample. For all of the three Pt-Ni octahedral nanoparticles, peaks corresponding to (111), (200) and (220) crystal planes are observed, while no diffraction peak corresponding to pure Pt or Ni is observed, indicates the formation of Pt-Ni alloy with the face-centered-cubic (fcc) structure. For all the Pt-Ni

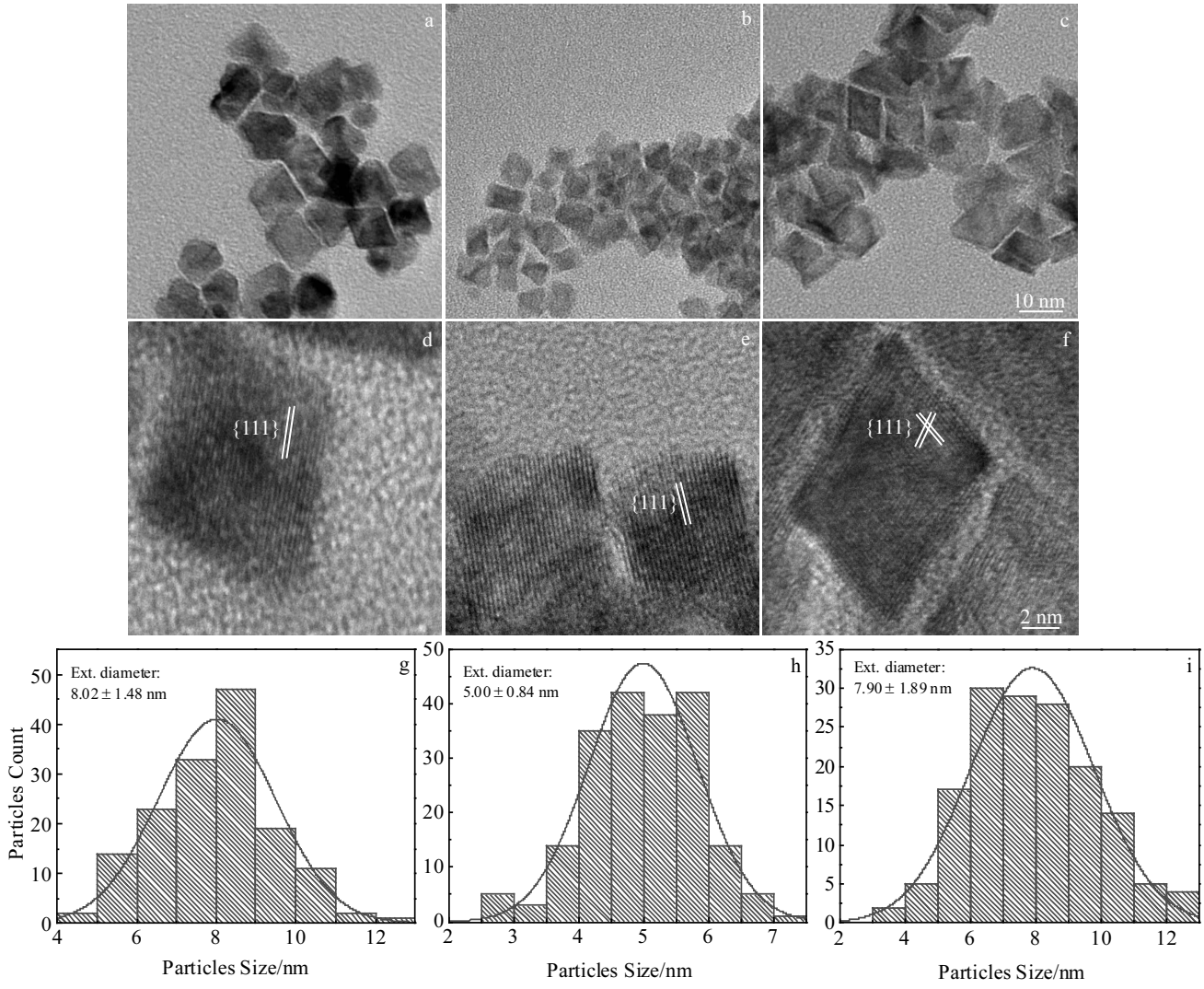

Fig.2 TEM (a~c), HRTEM (d~f) images and particle size distribution (g~i) of PtNi nanoparticles synthesized with different Pt:Ni atomic ratios: (a, d, g) 3:1; (b, e, h) 1:1; (c, f, i) 1:2

octahedral nanoparticles, the (111) peaks are shifted toward higher 2θ value compared with Pt (111), indicating that the Pt-Pt distance is shortened by the formation of Pt-Ni alloy, in agreement with the results from HRTEM. Small shoulder peaks appearing at lower 2θ value suggests the Pt segregation on the surface. The crystallinity of Pt_3Ni octahedral nanoparticles is higher than that of PtNi and $PtNi_2$, as indicated from the peak intensity in Fig.3b. From Fig.3b, it can also be observed that the 2θ value of the (111) peak is in the order of Pt_3Ni>$PtNi_2$>PtNi. Based on Bragg's law, the higher 2θ value means lower *d*-spacing, and thus the results from XRD coincide with that from TEM with the *d*-spacing order of Pt_3Ni<$PtNi_2$<PtNi. The positive shift of the diffraction peak indicates the contraction of surface lattice[18,19], which results in the downshift of the *d*-band center of Pt[19,20]. As a result, the strength of Pt-O band is weakened. As illustrated by the density functional theory (DFT) calculation, the optimum ORR catalysts should adsorb the oxygen species around 0.2 eV weaker than that on Pt(111)[21]. In our study, the oxygen species adsorbed on all three Pt-Ni octahedral nanoparticles are weakened by surface contraction, resulting in enhanced ORR activity compared with Pt/C. What's more, the extent of surface contraction is in the order of Pt_3Ni>$PtNi_2$>PtNi as indicated by XRD, which explains the "crater plot" trend of ORR activity.

2.3 Surface electronic properties of the as-synthesized Pt-Ni nanoparticles

XPS was adopted to further investigate the surface property of as-synthesized Pt-Ni octahedral nanoparticles as demonstrated in Fig.4. The binding energy (BE) of Pt in all the Pt-Ni samples is shifted to higher energy. As previously reported, the upshift of BE implies a downshift of d-band center of Pt,

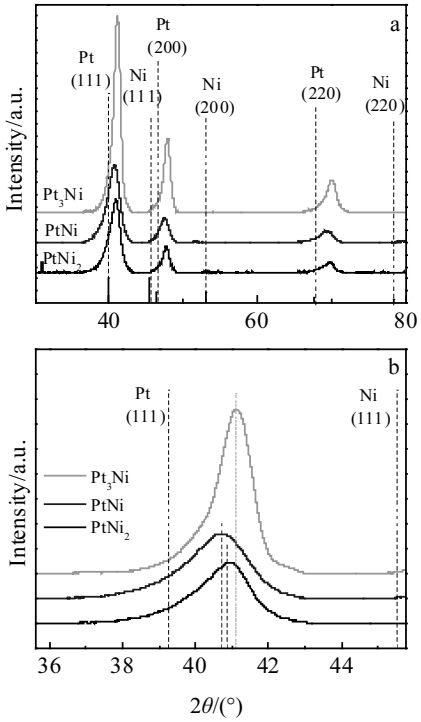

Fig.3 XRD patterns of PtNi nanoparticles synthesized with different Pt:Ni atomic ratios: (a) 2θ=30°~75° and (b) 2θ=35°~46°

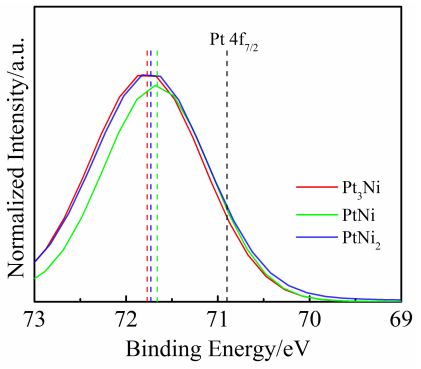

Fig.4 Area normalized Pt $4f_{7/2}$ XPS spectra of PtNi nanoparticles synthesized with different Pt:Ni atomic ratios

resulting in the weakened Pt-O bond[22]. The upshift trend of BE is shown in Fig.4, and the result confirms the former discoveries in TEM and XRD. As j_s is normalized to the surface Pt area, j_s is always considered as the instinct activity of the catalyst, which is related to the morphology and surface structure. Therefore, the value of j_s should be directly related to the surface properties such as surface contraction. While considering the cost, j_m is more realistic, which is determined by both the instinct activity and the Pt utilization. The relationship of j_m, j_s and ECSA (calculated from Fig.1a), can be described as below:

$$j_m(\mathrm{mA/mg_{Pt}}) = \mathrm{ECSA(cm^2/mg_{Pt})} \times j_s(\mathrm{mA/cm^2}) \quad (3)$$

Table 1 Pt:Ni atomic ratio of near-surface, bulk and the Pt utilization

	Pt_3Ni	PtNi	$PtNi_2$
Near-surface	0.71/0.29	0.64/0.36	0.53/0.47
Bulk	0.73/0.27	0.53/0.47	0.34/0.66
Pt utilization	0.97	1.21	1.56

From Eq.(3), it is clear that the j_m can be increased by enlarging the ECSA, which explains the enhancement in j_m of PtNi and $PtNi_2$ due to their high ECSA, regardless of their relatively low j_s. Table 1 lists the Pt:Ni atomic ratio of near-surface and bulk, which is calculated form results of XPS (Fig.4) and ICP-AES, respectively. With the increasing atomic ratio of Ni in bulk, the Pt utilization (defined as near-surface Pt at% divided by bulk Pt at%) is increased accordingly. This increases ECSA and enhances j_m of the Pt-Ni nanoparticles with the high bulk Ni atomic ratio.

3 Conclusions

1) Here we studied the ORR activities of Pt-Ni octahedral nanoparticles with Pt:Ni atomic ratio of 1:2, 1:1 and 3:1.

2) The results of structural characterization suggest that the extent of surface lattice contraction is affected by the Pt:Ni atomic ratio, which is considered as a key factor that can influence the absorption/desorption strength of the O-species on Pt surface.

3) The kinetics of ORR is controlled by the adsorption/desorption strength of the surface species, and the ORR activity is directly related to the surface contraction caused by Ni incorporation. The different extent of surface contraction is determined by the Pt:Ni ratio, and thus the “crater plot” relationship between the Pt:Ni atomic ratio and ORR activity can be explained.

References

1 Wu J B, Zhang J L, Peng Z M *et al*. *Journal of the American Chemical Society*[J], 2010, 132: 4984
2 Zhang J, Yang H Z, Fang J Y *et al*. *Nano Letters*[J], 2010, 10(2): 638
3 Chen L M, Ma D, Zhang Z *et al*. *Catalysis Letters*[J], 2012, 142(8): 975
4 Cui C, Gan L, Li H H *et al*. *Nano Letters*[J], 2012,12(11): 5885
5 Guo S, Li D, Zhu H *et al*. *Angew Chem Int Ed Engl*[J], 2013, 52(12): 3465
6 Alia S M, Pylypenko S, Neyerlin K C *et al*. *ACS Catalysis*[J], 2014, 4(8): 2680
7 Wu Z Y, Zhang W W, Sun S R. *Computational Materials Science*[J], 2016, 125: 278
8 Xiong Y L, Ma Y L, Lin Z Q *et al*. *Crystengcomm*[J], 2016, 18(40): 7823
9 Zhang Z C, Luo Z M, Chen B *et al*. *Advanced Materials*[J], 2016, 28(39): 8712

10 Liu T Y, Wang K, Yuan Q *et al*. *Nanoscale*[J], 2017, 9(9): 2963
11 Wang L, Gao W, Liu Z *et al*. *ACS Catalysis*[J], 2018, 8(1): 35
12 Stamenkovic V R, Fowler B, Mun B S *et al*. *Science*[J], 2007, 315(5811): 493
13 Choi S I, Xie S, Shao M *et al*. *Nano Letters*[J], 2013, 13(7): 3420
14 Cui C, Gan L, Heggen M *et al*. *Nat Mater*[J], 2013, 12: 765
15 Chao W, Rao R R, Peng J *et al*. *Advanced Materials*[J], 2019, 31: 1 806 296
16 Gilman S. *Journal of Electroanalytical Chemistry*[J], 1964, 7(5): 382
17 Carpenter M K, Moylan T E, Kukreja R S *et al*. *Journal of the American Chemical Society*[J], 2012,134(20): 8535
18 Wu J, Gross A, Yang H. *Nano Lett*[J], 2011, 11(2): 798
19 Luo L, Zhu F, Tian R *et al*. *ACS Catalysis*[J], 2017, 7(8): 5420
20 Chen Y, Liang Z, Yang F *et al*. *The Journal of Physical Chemistry C*[J], 2011, 115(49): 24 073
21 Greeley J, Stephens I E L, Bondarenko A S *et al*. *Nat Chem*[J], 2009, 1(7): 552
22 Wakisaka M, Mitsui S, Hirose Y *et al*. *The Journal of Physical Chemistry B*[J], 2006, 110(46): 23 489

Pt:Ni 原子比对 Pt-Ni 八面体氧还原活性的影响

段　骁[1]，黄　龙[1]，栗云彦[1]，唐　玲[1]，卢　军[1]，赵云昆[2]，刘　锋[1]

(1. 云南省贵金属新材料控股集团有限公司，云南 昆明 650106)

(2. 昆明贵研催化剂有限责任公司 贵金属催化技术与应用国家地方联合工程实验室，云南 昆明 650106)

摘　要：Pt-Ni 八面体纳米颗粒被认为是具有开发前景的氧还原反应（ORR）催化剂。在之前的报道中 Pt-Ni 八面体氧还原活性随 Pt:Ni 原子比的变化往往被表述为火山曲线，并缺乏相关的构效关系研究。本实验通过对不同 Pt:Ni 原子比的 Pt-Ni 八面体纳米粒子 ORR 性能表征，发现了不同于先前报道的 ORR 面积比活性与 Pt:Ni 原子比的关系：Pt_3Ni>$PtNi_2$>PtNi。同时，在相同的 Pt 负载量下，ORR 质量比活性的大小顺序为 Pt_3Ni≈$PtNi_2$>PtNi。此反常的相互关系可以利用晶格收缩程度和 Pt 利用率进行解释：表面晶格收缩程度 Pt_3Ni>$PtNi_2$>PtNi，这与 ORR 面积比活性的顺序一致，而质量比活性同时受面积比活性与表面铂利用率的影响。以上结果证实 ORR 活性可以通过表面张力和铂利用率进行调变。

关键词：氧还原反应；Pt-Ni 八面体；原子比；表面晶格收缩；Pt 利用率

作者简介：段　骁，男，1990 年生，硕士，云南省贵金属新材料控股集团有限公司，云南 昆明 650106，电话：0871-68316562，E-mail: xiao.duan@spmcatalyst.com